European Heart Journal - Cardiovascular Imaging Advance Access published March 3, 2014

European Heart Journal – Cardiovascular Imaging
doi:10.1093/ehjci/jeu019

Three-dimensional rotational angiography fused with multimodal imaging modalities for targeted endomyocardial injections in the ischaemic heart

Dieter Frans Dauwe[1], Dieter Nuyens[1], Stijn De Buck[1], Piet Claus[2], Olivier Gheysens[3], Michel Koole[3], Walter Coudyzer[4], Nina Vanden Driessche[1], Laurens Janssens[1], Joris Ector[1], Steven Dymarkowski[4,5], Jan Bogaert[4,5], Hein Heidbuchel[1], and Stefan Janssens[1]*

[1]Department of Cardiovascular Sciences, Clinical Cardiology, KULeuven, Leuven, Belgium; [2]Department of Cardiovascular Sciences, Imaging and Cardiovascular Dynamics, KULeuven, Leuven, Belgium; [3]Department of Imaging and Pathology, Nuclear Medicine and Molecular Imaging, KULeuven, Leuven, Belgium; [4]Clinical Radiology, Gasthuisberg University Hospitals Leuven, Leuven, Belgium; and [5]Department of Imaging and Pathology, Translational MRI, KULeuven, Leuven, Belgium

Received 14 December 2013; accepted after revision 15 January 2014

Aim Biological therapies for ischaemic heart disease require efficient, safe, and affordable intramyocardial delivery. Integration of multiple imaging modalities within the fluoroscopy framework can provide valuable information to guide these procedures. We compared an anatomo-electric method (LARCA) with a non-fluoroscopic electromechanical mapping system (NOGA®). LARCA integrates selective three-dimensional-rotational angiograms with biplane fluoroscopy. To identify the infarct region, we studied LARCA-fusion with pre-procedural magnetic resonance imaging (MRI), dedicated CT, or ^{18}F-FDG-PET/CT.

Methods and results We induced myocardial infarction in 20 pigs by 90-min LAD occlusion. Six weeks later, we compared peri-infarct delivery accuracy of coloured fluospheres using sequential NOGA®- and LARCA-MRI-guided vs. LARCA-CT- and LARCA-^{18}F-FDG-PET/CT-guided intramyocardial injections. MRI after 6 weeks revealed significant left ventricular (LV) functional impairment and remodelling (LVEF 31 $\pm$ 3%, LVEDV 178 $\pm$ 15 mL, infarct size 17 $\pm$ 2% LV mass). During NOGA®-procedures, three of five animals required DC-shock for major ventricular arrhythmias vs. one of ten during LARCA-procedures. Online procedure time was shorter for LARCA than NOGA® (77 $\pm$ 6 vs. 130 $\pm$ 3 min, $P < 0.0001$). Absolute distance of injection spots to the infarct border was similar for LARCA-MRI (4.8 $\pm$ 0.5 mm) and NOGA® (5.4 $\pm$ 0.5 mm). LARCA-CT-integration allowed closer approximation of the targeted border zone than LARCA–PET (4.0 $\pm$ 0.5 mm vs. 6.2 $\pm$ 0.6 mm, $P < 0.05$).

Conclusion Three-dimensional -rotational angiography fused with multimodal imaging offers a new, cost-effective, and safe strategy to guide intramyocardial injections. Endoventricular procedure times and arrhythmias compare favourably to NOGA®, without compromising injection accuracy. LARCA-based fusion imaging is a promising enabling technology for cardiac biological therapies.

Keywords Endomyocardial injections • Ischaemic heart failure • Rotational angiography • Cardiac magnetic resonance imaging • Cell transplantation • Cardiac computed tomography • Cardiac positron emission tomography

Introduction

Development of protein- and cell-based therapy for advanced ischaemic heart disease requires efficient and widely applicable intramyocardial delivery strategies. To date, the NOGA®-platform (Biosense Webster) is a reference technique to guide percutaneous intramyocardial injections of biologicals into the ischaemic

* Corresponding author: Department of Cardiovascular Diseases, Gasthuisberg University Hospitals Leuven, Herestraat 49, 3000 Leuven, Belgium. Tel: +32 16344235; Fax: +32 16344240, Email: stefan.janssens@med.kuleuven.be

myocardium.[1–4] NOGA® is able to differentiate regions of non-viable, viable ischaemic/hibernating, and viable healthy myocardium, based on real-time acquisition of a three-dimensional (3D) endoventricular electromechanical map.[5–7] NOGA®-guided injection strategies are thus based on real-time functional data (both endocardial potential and regional contraction). This strategy requires considerable experience, is costly, provides only limited anatomical feedback and may have less discriminatory power in identifying non-transmural scar areas.[8] Injection strategies based on structural feedback could thus offer a promising alternative.

Magnetic resonance imaging (MRI) allows unparallelled myocardial tissue contrast discrimination but the need for complex XMR-facilities and MRI-compatible, coiled endovascular catheters remain obstacles.[9,10] The possibility of integrating pre-procedural MRI images with live X-ray fluoroscopy circumvents these limitations.[11] Alternatively, the location and extent of the infarct region could be derived from computed tomography (CT) or ^{18}F-FDG positron emission tomography (PET) in MRI-incompatible patients.

Here, we report the safety, feasibility, and accuracy of a novel mapping technique as an extension to our leuven augmented reality catheter ablation system (LARCA) currently used in our centre to guide electrophysiological ablation procedures in all heart chambers.[12] LARCA integrates selective 3D rotational angiograms (3D-RA) with live biplane fluoroscopy in an augmented reality environment. To guide endomyocardial injections towards the infarct border zone, left ventricular (LV)-3D-RAs were integrated with manual infarct delineations, derived from pre-procedural imaging modalities (MRI, CT, or PET/CT). This methodology was investigated in a non-inferiority comparative study with the NOGA®-platform.

Methods

Study design

The study was approved by the Ethics Committee for Animal Experimentation (KULeuven, Belgium), and was performed in accordance with the Guide for Care and Use of Laboratory Animals (NIH). MRI, dedicated CT, or ^{18}F-FDG-PET/CT was performed 6 weeks after infarct induction. Fluorescent microspheres were injected 4 ± 1 days after image acquisition. In a first set of five animals, head-to-head comparison between a NOGA® and LARCA-MRI-guided injection strategy was performed. In a second set of experiments, we injected three animals using LARCA-CT-integration and three animals using LARCA-^{18}F-FDG-PET/CT-integration (*Figure 1*). All animals were euthanized by i.v. propofol overdose and oversaturated potassium chloride.

Infarct induction

Domestic pigs, weighing 25–30 kg, were pre-medicated with amiodarone 400 mg daily from Day −14 to −7 and 200 mg daily from Day −7 until infarct induction. Pre-treatment with aspirin 300 mg and clopidogrel 300 mg was initiated at Day −1. Pigs were pre-anaesthetized with tiletamine/zolazepam (8 mg/kg i.m.) and xylazine hydrochloride (2.5 mg/kg i.m.), followed by a continuous infusion of propofol (10 mg/kg/h) and remifentanil (0.3 μg/kg/min). The animals were intubated and ventilated with a 1 : 1 mixture of air and oxygen. Invasive blood pressure and ECG were monitored during the whole procedure. Myocardial infarction was induced in 20 pigs using a 90-min stented balloon inflation in the proximal left anterior descending coronary artery (2.5–3.5 × 8, Presilion Plus, Cordis®). Aspirin and clopidogrel daily treatment was continued until euthanasia 6 weeks later.

MRI cine-angiography and delayed enhancement

Cardiac MRI (3 T Siemens® Trio) was performed 6 weeks after infarct induction using the Siemens Numaris-4 software, ECG-triggering, and cardiac-dedicated surface coils. The LV was completely encompassed

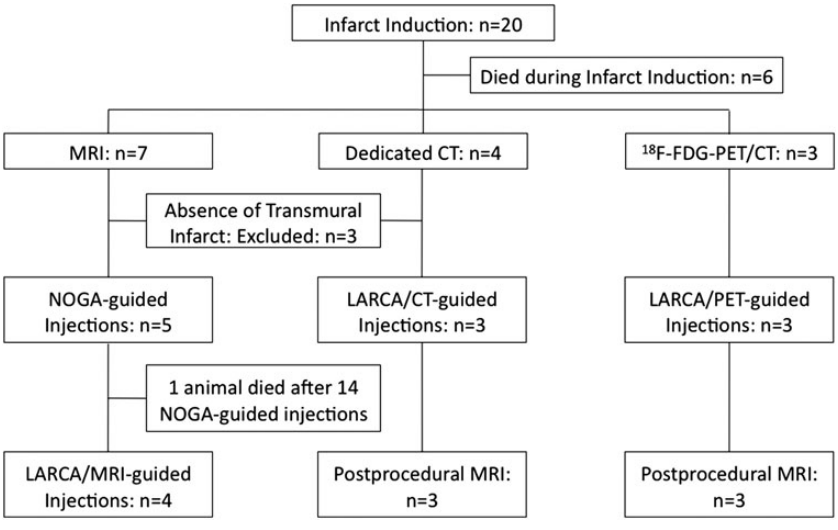

Figure 1: Experimental study design: a total of 20 pigs were infarcted. Endomyocardial injections were performed both by NOGA® and LARCA-MRI-guidance in four pigs. In an additional subset of six animals, three pigs were injected using LARCA-CT-guidance and another three pigs using LARCA-PET-guidance.

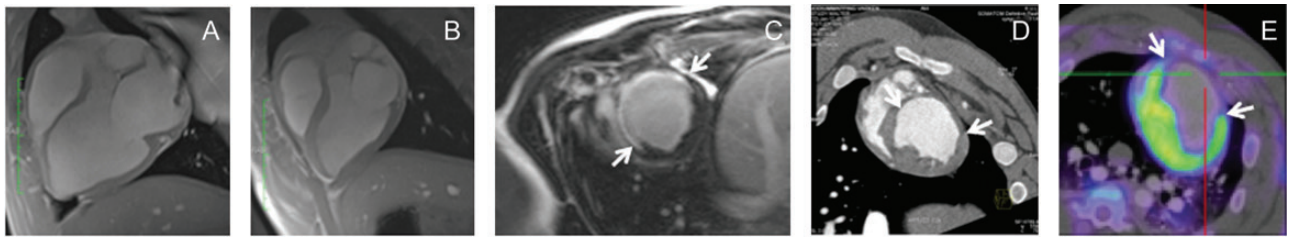

Figure 2: Identification of the infarct region on pre-procedural imaging: 6 weeks after myocardial infarction, cine-MRI images at end-diastole demonstrate important LV-dilatation and anteroseptal wall thinning (*A*) in comparison with sham animals (*B*). The infarct region is clearly identified between arrows on MRI-delayed enhancement (*C*), dedicated CT (*D*) and ^{18}F-FDG-PET/CT short-axis views (*E*).

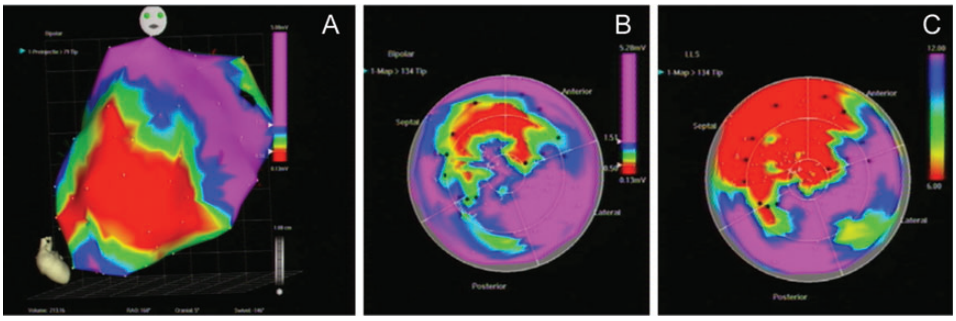

Figure 3: NOGA®-map: 3D BPV map (*A*) and corresponding bull's eye plots representing BPV (*B*) and LLS (*C*). The different injection spots in the peri-infarct border are indicated as black dots on the bull's eye representations. Injections were directed towards the peri-infarct border region based on a BPV between 0.5 and 1.5 mV.

by contiguous 6-mm thick short-axis slices, and global function and infarct area (*Figure 2A–C*) analysed as described previously.[13]

Dedicated CT

Cardiac 128-slice CT (Siemens Somatom Definition Flash, Siemens® AG, Erlangen, Germany) was performed 6 weeks after infarct induction. CT was acquired after i.v. administration of 60 mL of a non-diluted iodine contrast agent at a rate of 5 mL/s. Bolus triggering was performed in the ascending aorta to initiate image acquisition (detector collimation: 128 × 0.6 mm, Voltage: 120 kV, tube current: 320 mAs). All studies were performed using ventilation-stop and ECG-triggering, allowing reconstruction of both systolic and diastolic phase of the cardiac cycle and infarct delineation based on transmural end-diastolic wall thickness (*Figure 2D*).

^{18}F-FDG-PET/CT

Six weeks after infarct induction, animals were fasted overnight and a hyperinsulinaemic euglycaemic clamp was performed before tracer injection and acquisition of ^{18}F-FDG-PET/CT.[14] Insulin (0.08 units/kg/h) was continuously infused and glycaemia was monitored every 2–5 min. Glucose 20%, supplemented with KCl (80 mEq/L), was administered to achieve a steady-state glycaemia between 70 and 110 mg/dL. Fifteen minutes thereafter, 370 MBq ^{18}F-FDG was injected i.v., followed by a low-dose CT scan for attenuation correction. A 60-min static PET-image of the myocardium was acquired 20 min later (HiRez Biograph 16, Siemens®, Knoxville) (*Figure 2E*). Images were reconstructed using OSEM.

NOGA®-mapping

Electro-mechanical maps, based on an average of 122 ± 13 mapping points encompassing the whole LV, were obtained with the NOGA®-system, using a Myostar® injection catheter (Biosense Webster). The infarct region was identified using stringent bipolar voltage (BPV $<$0.5 mV) and local linear shortening (LLS) criteria. Regions with preserved linear shortening and BPV $>$1.5 mV were defined as healthy myocardium (*Figure 3*).

LARCA

Pre-procedural MRI, CT, and PET images were manually delineated on an offline workstation to obtain segmentation surfaces for endocard, aortic arch, and myocardial infarct region, corresponding to the cardiac phase resembling interventional LV-3D-RA. For MRI-delayed-enhanced imaging, non-rigid image registration techniques were applied to transform the infarct surface to the interventional reference phase. Hence a single phase 3D LV-model is obtained, reflecting wall thickness, infarct size, and infarct location. During the intervention, a LV-3D-RA was acquired with a single C-arm rotation, as reported before.[15] Combined rapid pacing in both right ventricle and right atrium (200 ms cycle length) was used to obtain a quasi cardiac standstill in order to reduce motion artefacts. Following online reconstruction of the 3D-dataset

obtained from the X-ray projection images, an endocast surface segmentation of the LV and aortic arch was generated. The latter LV-surface was registered with the corresponding MRI, CT, or PET-based LV-segmentation, using an iterative closest points-like (ICP) surface registration technique.[16] This approach resulted in a detailed, high-resolution 3D endocardial surface model, including MRI, CT, or PET-derived information about wall thickness and infarct location in a single co-ordinate system. This model was subsequently integrated with and semi-transparently projected on live biplane orthogonal fluoroscopy images, as previously described.[12,17] The resulting augmented reality visualization was presented to the operator on two monitors in the catheterization laboratory, hence providing real-time feedback to safely navigate the catheter towards the infarct border (*Figure 4*) *(*Supplementary data online, *Video S1)*.

Intramyocardial injections

A pre-defined goal of 20 injections of 200 μL fluorescently labelled microspheres was performed 6 weeks after infarct induction using the Myostar® injection catheter (Biosense Webster). Needle length was adjusted to 3–4 mm, depending on the wall thickness of the peri-infarct border, assessed by pre-procedural MRI, CT, or PET.

In an initial set of five animals, injections of orange fluospheres (Invitrogen®, 18 ± 1 spots/animal) were delivered using NOGA®-guidance, followed by LARCA-MRI-guided injections of green fluospheres (19 ± 1 spots/animal). NOGA®-guided endomyocardial injections were directed towards the peri-infarct border region based on a BPV between 0.5 and 1.5 mV (*Figure 3*). LARCA-MRI-guided endomyocardial injections were directed towards the peri-infarct border region, identified from pre-procedural late-enhanced MRI (*Figure 2C*).

In additional six animals, endomyocardial injections were delivered using LARCA-CT ($n = 3$;17 ± 2 spots/animal) or LARCA-^{18}F-FDG-PET/CT ($n = 3$; 20 ± 0 spots/animal) integration. Infarct delineation was based on end-diastolic wall thinning (*Figure 2D*) in the former and ^{18}F-FDG uptake (*Figure 2E*) in the latter group of animals.

Processing and analysis

After euthanasia, the heart was embedded in 5% agarose solution, sectioned in contiguous 5-mm slices from the apex to the base, and stained with 2,3,5-triphenyltetrazolium chloride (TTC) allowing infarct identification. All slices were photographed under normal and UVA light on both sides and pictures subsequently co-registered to obtain an *ex vivo* 3D-stack of the LV (Supplementary data online, *Figure S1)*. TTC-defined infarct border, together with endocardial and epicardial surfaces were manually delineated. UVA-illumination allowed localization and differentiation of orange and green fluosphere injection spots. The distance from endomyocardial injection spots towards the TTC-defined infarct border was semi-automatically quantified in a 3D co-ordinate system and injection accuracy was compared in the apical, mid, and basal third of the LV.

Statistical analysis

All data are presented as means ± SEM. Intergroup differences were analysed using two-tailed unpaired *t*-tests. $P < 0.05$ was considered

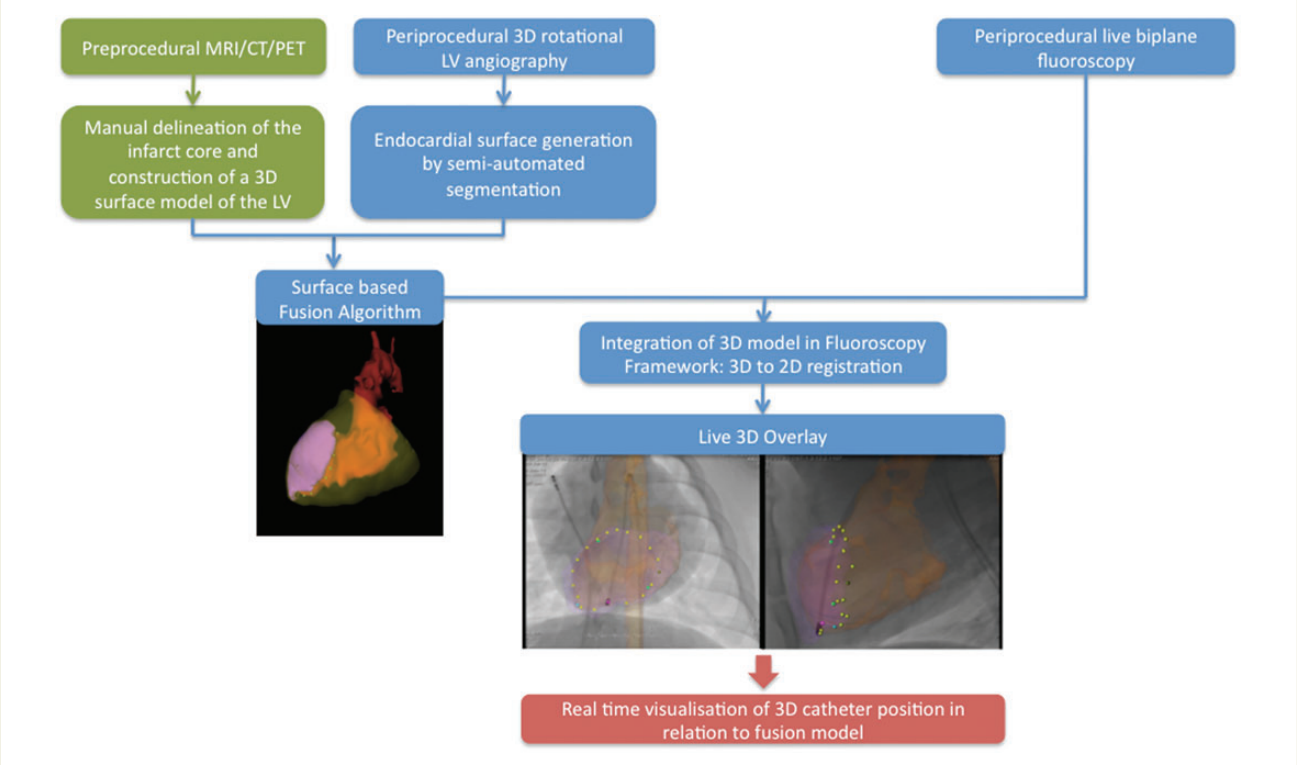

Figure 4: LARCA-algorithm: pre-procedural infarct and endocard delineations are registered with a periprocedurally acquired 3D rotational angiography using a surface based fusion algorithm. The resulting 3D-model is presented to the operator as a semi-transparent overlay on conventional live biplane fluoroscopy in an orthogonal configuration. The tasks indicated in green are completed pre-procedurally, while the tasks indicated in blue are performed during the intervention.

statistically significant. All analyses were performed with Prism 5.0a (GraphPad Software, Inc.).

Results

Animal model

Myocardial infarction was induced in 20 animals, of which 14 survived to 6 weeks. The rise in troponin-I and CK-Mb at 2 h reperfusion was 560 ± 77 (≤0.13) and 122 ± 43 μg/L (≤3.5), respectively. Following MRI or CT analysis at 6 week follow-up, three pigs were excluded because of limited myocardial infarction. In comparison with sham animals ($n = 3$), cine-MRI at 6 weeks confirmed significant functional impairment and LV-remodelling in the infarcted pigs ($n = 11$): LVEF 31 ± 3%, LVEDV 178 ± 15 mL, and LVESV 122 ± 10 mL (*Table 1*). The region of delayed enhancement composed 17 ± 2% of the total LV-mass. LV-volumes obtained by MRI correlated closely to the volumes assessed by NOGA® in the subset of animals undergoing NOGA®-guided injection procedures ($n = 5$): LVEF 31 ± 1%, LVEDV 199 ± 11 and LVESV 138 ± 9 mL.

Intramyocardial injections

In the first series of experiments, an average of 18 ± 1 injections per pig were delivered using NOGA®, whereas 19 ± 1 injections were delivered afterwards in the same animals using LARCA-MRI. Electrical irritability of some peri-infarct regions in two of five animals precluded to deliver the pre-defined number of 20 injections, equally distributed around the infarct. In total, 89 and 75 injections were delivered using NOGA® and LARCA-MRI respectively, of which 49 NOGA®-guided injection spots (55%) and 42 LARCA-MRI-guided injection spots (56%) could be localized in the 5 mm thick ventricular tissue slices. LARCA-MRI and NOGA® enabled spatial confinement of >90% of injection spots <1 cm from the targeted infarct border (*Table 2*). The mean absolute distance of the injection spots to the infarct border was 4.8 ± 0.5 and 5.4 ± 0.5 mm for LARCA-MRI and NOGA®, respectively, $P = 0.40$ (*Figure 5*). We also analysed the mean signed distance, with negative values representing localizations towards the infarct core, and positive values representing localizations at the opposite side of the infarct border, towards remote myocardium. The mean signed distance of the injection spots to the TTC-defined infarct border was −0.6 ± 0.9 mm for NOGA® and −2.3 ± 0.8 mm for LARCA-MRI-guided injections, $P = 0.19$ (*Figure 6*).

In an additional six animals, a total of 52 and 60 injections were delivered utilizing LARCA-CT or LARCA-PET, respectively. Induction of sustained VT and VFib after 13 injections precluded to deliver a pre-defined goal of 20 injections in one animal, injected using LARCA-CT-guidance. In total, 32 LARCA-CT (62%)- and 44 LARCA-PET (73%)-guided injection spots could be localized *ex vivo*. Delivery using LARCA-CT-integration allowed the closest

Table 1 MRI-data 6 weeks after myocardial infarction

MRI	LVEDV (mL)	LVESV (mL)	LVEF (%)	DE (% LV)
Sham ($n = 3$)	116 ± 6	48 ± 2	58 ± 4	0
6w post MI ($n = 11$)	178 ± 15[a]	122 ± 10[a]	31 ± 3[a]	17 ± 2[a]

Six weeks after myocardial infarction, MRI-analysis demonstrates important functional impairment and LV-remodelling in comparison with sham animals.
[a] *P*-value <0.05.

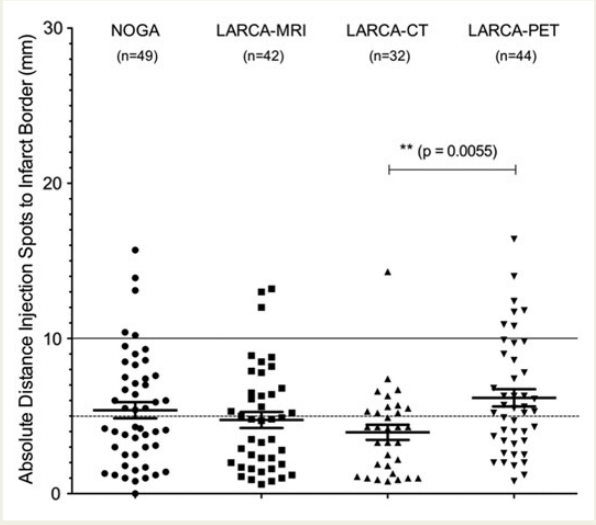

Figure 5: Absolute distance of the injection spots to the infarct border: absolute distance of the different injection spots to the TTC-defined infarct border. These values do not take into account whether the injections are localized at the infarcted or remote side of the targeted infarct border.

Table 2 Injection accuracy and depth

	NOGA	LARCA-MRI	LARCA-CT	LARCA-PET
Injections ≤5 mm of infarct border (% total)	51%	60%	66%	43%
Injections ≤10 mm of infarct border (% total)	90%	93%	97%	84%
Average injection depth (mm)	2.5 ± 0.3	2.9 ± 0.4	3.2 ± 0.4	2.7 ± 0.4
Average wall thickness (mm)	9.1 ± 0.4	9.7 ± 0.5	10.1 ± 0.6	8.8 ± 0.4

Percentage of the injection spots localized ≤5 and ≤10 mm of the targeted infarct border (absolute distance). Average injection depth and average post-mortem wall thickness at the corresponding injection localizations.

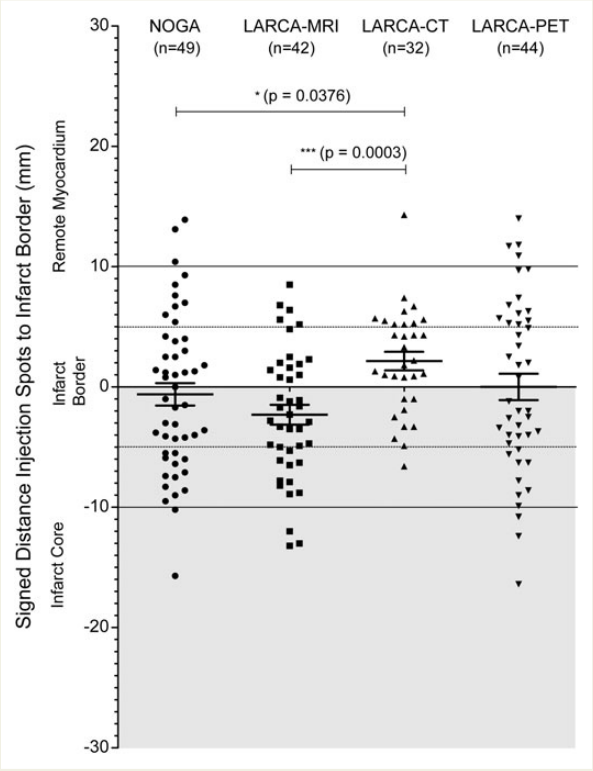

Figure 6: Signed distance of the injection spots to the infarct border: signed distance of the different injection spots to the TTC-defined infarct border. Negative values represent localizations at the infarcted side of the infarct border, whereas positive values represent injections at the opposite side, towards remote myocardium.

approximation of the targeted infarct border zone with the smallest distribution between the different injection spots (*Figure 5*). The mean absolute distance to the infarct border was 4.0 ± 0.5 mm for LARCA-CT-guided injection spots and 6.2 ± 0.6 mm for LARCA-PET-guided injection spots, $P = 0.006$ (*Figure 5*). Moreover, 97% of all LARCA-CT-guided injections and 84% of all LARCA-PET-guided injections were localized <1 cm from the infarct border (*Table 2*).

In comparison with NOGA® ($P = 0.038$) and LARCA-MRI ($P = 0.0003$), LARCA-CT-guided injections were clustering more outside the actual infarct core towards remote, non-ischaemic myocardium (*Figure 6*). The mean signed distance of the injection spots to the infarct border was 2.2 ± 0.8 mm for LARCA-CT-guided injections and 0.0 ± 1.1 mm for LARCA-PET-guided injections.

Obtaining perpendicular wall contact and a stable catheter position was more challenging for endomyocardial injection targets localized at the base of the LV. This was confirmed by regional differences in injection efficiency. For all LARCA-modalities combined, only 36.7% of the planned targets localized at the base of the LV could be identified on post-mortem sections. In comparison, 66.7% of the apical and 64.6% of the mid-ventricular targets could be localized *ex vivo* (Supplementary data online, *Table S1*). Despite the difficulties to obtain a stable catheter position for intramyocardial delivery at the base of the LV, targeting accuracy remained unchanged if such a position could actually be achieved (Supplementary data online, *Figure S2*).

No differences were noted in injection depth between the different guiding strategies (*Table 2*, Supplementary data online, *Figure S3*). Average *ex vivo* defined injection depth was 2.8 ± 0.2 mm. Average post-mortem transmural wall thickness at the corresponding injection sites was 9.4 ± 0.2 mm. More than 84% of the injections were localized in the inner 50% of the total wall thickness, with a median injection depth corresponding to 23% endo-epicardial transmurality.

During NOGA®-procedures, three of five animals required DC-shock for major ventricular arrhythmias vs. one of ten during LARCA-procedures. One animal died after 14 NOGA®-guided injections, due to intractable VFib. None of the animals showed signs of ventricular perforation, pericardial tamponade, intramural hematomas, aortic valve injury, or aortic/coronary dissection during careful post-mortem examination. Average cardiac marker release, 2 h after 20 intramyocardial injections, was 2.38 ± 0.22 μg/L for troponin-I (≤0.13) and 4.5 ± 0.9 μg/L for CK-Mb (≤3.5).

Online procedure time was significantly shorter for LARCA-procedures in comparison with NOGA®. Introduction of pacing catheters, acquisition of a LV-3D-RA and subsequent online fusion with pre-procedural MRI, CT, or PET datasets accounted for 46 ± 6 min. Average procedure time for LARCA-guided injections was 31 ± 4 min. A NOGA®-map, encompassing the whole LV (122 ± 13 mapping points), was reconstructed in 75 ± 5 min. Subsequent procedure time for NOGA®-guided injections was 55 ± 4 min. This accounted for a total online procedure time of 77 ± 6 min for LARCA vs. 130 ± 4 min for NOGA®, $P < 0.0001$.

Discussion

We report a novel mapping strategy to guide endomyocardial injections into the infarcted heart, offering a safe, fast, and accurate alternative to existing non-fluoroscopic electromechanical mapping systems. LARCA-guidance is based on in-house developed fusion of pre-procedural multimodal imaging of the heart with 3D-RA during radiofrequency catheter ablation (LARCA). In this study, we characterized the use of this anatomo-electric approach for targeted injections of fluorescent microspheres in the infarct border zone. We observed less arrhythmic side-effects and shorter online procedure times than the electromechanical mapping standard NOGA®, without compromizing on injection accuracy. Both LARCA-MRI and NOGA® enabled spatial confinement of >90% of injection spots <1 cm from the targeted infarct border. The median injection depth did not extend beyond the endocardial 25% of the total LV-wall transmurality, a pre-requisite for safe intramyocardial delivery in ischaemic heart disease.

Acquisition of a LV-3D-RA integrated with pre-procedural multimodal imaging obviates the need for multiple and prolonged endocardial contact time, as required to construct a complete NOGA®-map. Hence, the risk of inducing ventricular arrhythmias in inherently vulnerable and irritable ischaemic myocardium was also significantly reduced, although the concomitant anti-arrhythmic beta-blocker and/or amiodarone use were not different between groups. Finally, since manual delineations are performed on an offline workstation prior to the procedure, they do not interfere with online procedure time, which is therefore significantly shorter.

Despite the highly dynamic environment of the LV, vast majority of the injections was localized within 1 cm of the targeted infarct border, irrespective of the fusion modality used. For the evaluation of targeting accuracy on post-mortem TTC-stained sections, the minimal slice thickness of 5 mm limited tissue penetration of UVA light, and hence reduced the number of identifiable injection spots. Of note, LARCA-CT-guided injections showed a greater clustering pattern towards healthy, remote myocardium. LARCA–PET-guided injections in contrast, showed a greater dispersion across the infarct border, potentially caused by the lesser spatial resolution and static/ungated acquisition of the PET-images obtained.

Delivery route is a major determinant of cell/protein retention in the injured myocardium. Transvascular cell administration has been mainly implemented in the (sub)acute phase after myocardial infarction, as it relies on up-regulation of cell adhesion molecules and homing signals for optimal retention. In contrast, in advanced ischaemic heart disease, the occurrence of collateral flow, severe coronary stenoses, and/or chronic total occlusions, together with loss of homing signals and down-regulation of adhesion molecules, limits intracoronary delivery efficiency. Hence, intramyocardial delivery has been proposed as the preferred delivery strategy. Whereas transepicardial injections are limited to patients scheduled for cardiac surgery, transendocardial injections offer a less invasive treatment strategy as a stand-alone procedure. To date, the NOGA®-platform is established as a reference technique to guide transendocardial injections into the ischaemic myocardium, allowing differentiation of ischaemic, viable myocardium, based on electromechanical mapping. Limited availability and experience with NOGA® throughout most cardiac centres, in combination with its considerable cost, hamper widespread clinical application of transendocardial injection strategies.

In contrast to NOGA®, our mapping strategy allows guidance of endomyocardial injections into ischaemic areas, based on anatomical and structural feedback, derived from imaging modalities readily available in most cardiac centres. Fusion of pre-procedural late-enhanced MRI images with a LV-3D-RA provides the operator a 3D-model with both high soft tissue contrast discrimination and high spatial resolution. In contrast to the work presented by de Silva *et al.*,[11] our algorithm allowed co-registration of the pre-procedural model within the fluoroscopy framework without the use of external fiducial markers. Accurate demarcation of viable from non-viable myocardium is critically important for safe and effective biological therapies aimed at enhancing cardiac repair. Our data indicate that this is also possible using pre-procedural CT or ^{18}F-FDG-PET/CT in an MRI-incompatible patient population.

In addition to providing highly detailed anatomical information, the system allows integration of functional feedback. Endocardial potentials and activation times, acquired during selective voltage mapping of a region of interest, can be transferred onto the 3D anatomical model.[17] This data can be presented to the operator as a colour-coded map on the surface of the model. Moreover, additional useful information, including MRI-derived regional contraction and wall thickness, could also be annotated to the model.

Some limitations need to be considered. First, LARCA does not eliminate the need for iodine contrast and X-ray imaging. The effective radiation dose to acquire a single 3D-RA is 6.6 $\pm$ 1.8 mSv, which can be reduced up to $\sim$1.2–2.6 mSv through manual collimation of the radiation beam and recent optimization of our 3D-RA-acquisition protocol.[18] In comparison, radiation doses for conventional, ungated cardiac CT range between 8.5 and 16 mSv for 16-slice, 32-slice or dual-source CT.[19,20] Secondly, integration of pre-procedural imaging and manual segmentation may increase cost, which needs to be evaluated against the investment in dedicated hardware and specialized catheters for existing electromechanical mapping systems. Thirdly, administration of rapid pacing requires general anaesthesia, but recent optimizations in 3D-RA acquisition have allowed to acquire these images during conventional slow pacing protocols.

In conclusion, LARCA-guided injection procedures in a clinically representative model of ischaemic heart disease were associated with equivalent injection accuracy, less arrhythmias, and shorter online procedure times then NOGA®. LARCA offers a new and promising strategy to accurately guide intramyocardial injections towards the peri-infarct region, based on technology and experience readily available in most cardiac centres. Since LARCA-technology does not rely on dedicated hardware or specialized, costly catheters, it offers a favourable alternative to existing electromechanical mapping systems, facilitating delivery of future biological therapies to patients with ischaemic heart disease.

Supplementary data

Supplementary data are available at *European Heart Journal – Cardiovascular Imaging* online.

Acknowledgements

The authors thank Biosense Webster and S. Kramer for providing the NOGA®-platform and concomitant support. The authors also would like to thank J. Adams for his aid and expert technical assistance.

Conflict of interest: H.H. is a member of the scientific advisory board of Biosense Webster, Inc., and Siemens Medical Solutions, and receives unconditional research grants through the University of Leuven from St Jude Medical, Medtronic, Biotronik, and Boston Scientific, Inc. S.D.B. and H.H. received research funding through the University of Leuven from Siemens Medical Solutions for unrelated research.

Funding

This work was supported by the Research Foundation Flanders (FWO) and a KULeuven Research Grant (PF\10\014).

References

1. Perin EC, Dohmann HF, Borojevic R, Silva SA, Sousa AL, Mesquita CT *et al.* Transendocardial, autologous bone marrow cell transplantation for severe, chronic ischemic heart failure. *Circulation* 2003;**107**:2294–302.
2. Losordo DW, Henry TD, Davidson C, Sup Lee J, Costa MA, Bass T *et al.* Intramyocardial, autologous CD34+ cell therapy for refractory angina. *Circ Res* 2011;**109**:428–36.
3. Smits PC, van Geuns RJ, Poldermans D, Bountioukos M, Onderwater EE, Lee CH *et al.* Catheter-based intramyocardial injection of autologous skeletal myoblasts as a primary treatment of ischemic heart failure: clinical experience with six-month follow-up. *J Am Coll Cardiol* 2003;**42**:2063–9.
4. Duckers HJ, Houtgraaf J, Hehrlein C, Schofer J, Waltenberger J, Gershlick A *et al.* Final results of a phase IIa, randomised, open-label trial to evaluate the percutaneous intramyocardial transplantation of autologous skeletal myoblasts in congestive heart failure patients: the SEISMIC trial. *EuroIntervention* 2011;**6**:805–12.
5. Gyongyosi M, Sochor H, Khorsand A, Gepstein L, Glogar D. Online myocardial viability assessment in the catheterization laboratory via NOGA electroanatomic

mapping: quantitative comparison with thallium-201 uptake. *Circulation* 2001;**104**: 1005–11.
6. Gyongyosi M, Khorsand A, Sochor H, Sperker W, Strehblow C, Graf S *et al.* Characterization of hibernating myocardium with NOGA electroanatomic endocardial mapping. *Am J Cardiol* 2005;**95**:722–8.
7. Wiggers H, Botker HE, Sogaard P, Kaltoft A, Hermansen F, Kim WY *et al.* Electromechanical mapping versus positron emission tomography and single photon emission computed tomography for the detection of myocardial viability in patients with ischemic cardiomyopathy. *J Am Coll Cardiol* 2003;**41**:843–8.
8. Wijnmaalen AP, van der Geest RJ, van Huls van Taxis CF, Siebelink HM, Kroft LJ, Bax JJ *et al.* Head-to-head comparison of contrast-enhanced magnetic resonance imaging and electroanatomical voltage mapping to assess post-infarct scar characteristics in patients with ventricular tachycardias: real-time image integration and reversed registration. *Eur Heart J* 2011;**32**:104–14.
9. Saeed M, Martin AJ, Lee RJ, Weber O, Revel D, Saloner D *et al.* MR guidance of targeted injections into border and core of scarred myocardium in pigs. *Radiology* 2006; **240**:419–26.
10. Krombach GA, Pfeffer JG, Kinzel S, Katoh M, Gunther RW, Buecker A. MR-guided percutaneous intramyocardial injection with an MR-compatible catheter: feasibility and changes in T1 values after injection of extracellular contrast medium in pigs. *Radiology* 2005;**235**:487–94.
11. de Silva R, Gutierrez LF, Raval AN, McVeigh ER, Ozturk C, Lederman RJ. X-ray fused with magnetic resonance imaging (XFM) to target endomyocardial injections: validation in a swine model of myocardial infarction. *Circulation* 2006;**114**: 2342–50.
12. Ector J, De Buck S, Huybrechts W, Nuyens D, Dymarkowski S, Bogaert J *et al.* Biplane three-dimensional augmented fluoroscopy as single navigation tool for ablation of atrial fibrillation: accuracy and clinical value. *Heart Rhythm* 2008;**5**: 957–64.
13. Dubois C, Liu X, Claus P, Marsboom G, Pokreisz P, Vandenwijngaert S *et al.* Differential effects of progenitor cell populations on left ventricular remodeling and myocardial neovascularization after myocardial infarction. *J Am Coll Cardiol* 2010;**55**: 2232–43.
14. Knuuti MJ, Nuutila P, Ruotsalainen U, Saraste M, Harkonen R, Ahonen A *et al.* Euglycemic hyperinsulinemic clamp and oral glucose load in stimulating myocardial glucose utilization during positron emission tomography. *J Nucl Med* 1992;**33**: 1255–62.
15. Ector J, De Buck S, Nuyens D, Rossenbacker T, Huybrechts W, Gopal R *et al.* Adenosine-induced ventricular asystole or rapid ventricular pacing to enhance three-dimensional rotational imaging during cardiac ablation procedures. *Europace* 2009;**11**:751–62.
16. Besl PJ. MHD. A method for registration of 3-D shapes. *IEEE Trans Pattern Anal Mach Intell* 1992;**14**:239–56.
17. Ector J, De Buck S, Adams J, Dymarkowski S, Bogaert J, Maes F *et al.* Cardiac three-dimensional magnetic resonance imaging and fluoroscopy merging: a new approach for electroanatomic mapping to assist catheter ablation. *Circulation* 2005;**112**: 3769–76.
18. De Buck S, Alzand BS, Wielandts JY, Garweg C, Phlips T, Ector J *et al.* Cardiac three-dimensional rotational angiography can be performed with low radiation dose while preserving image quality. *Europace* 2013;**15**:1718–24.
19. Einstein AJ, Moser KW, Thompson RC, Cerqueira MD, Henzlova MJ. Radiation dose to patients from cardiac diagnostic imaging. *Circulation* 2007;**116**:1290–305.
20. Rixe J, Conradi G, Rolf A, Schmermund A, Magedanz A, Erkapic D *et al.* Radiation dose exposure of computed tomography coronary angiography: comparison of dual-source, 16-slice and 64-slice CT. *Heart* 2009;**95**:1337–42.